Angularly resolved two-photon above-threshold ionization of helium

Diego I. R. Boll, Omar A. Fojón, C. W. McCurdy, and Alicia Palacios

Phys. Rev. A **99**, 023416 — Published 14 February 2019

DOI: 10.1103/PhysRevA.99.023416

Angularly resolved two-photon above threshold ionization of helium

Diego I. R. Boll,[1] Omar A. Fojón,[2] C. W. McCurdy,[3,4] and Alicia Palacios[5,6,*]

[1] *Departamento de Química, Modulo 13, Universidad Autónoma de Madrid, 28049 Madrid, SPAIN*
[2] *Instituto de Física Rosario, CONICET-UNR, Blvd. 27 de Febrero 210 bis, 2000 Rosario, Argentina*
[3] *Lawrence Berkeley National Laboratory, Chemical Sciences, Berkeley, CA 94720*
[4] *Department of Chemistry, University of California, Davis, CA 95616*
[5] *Departamento de Química, Modulo 13, Universidad Autónoma de Madrid (UAM) 28049 Madrid, SPAIN*
[6] *Institute of Advanced Research in Chemical Sciences (IAdChem), UAM, 28049 Madrid, SPAIN*

(Dated: January 16, 2019)

Angularly resolved two-photon single ionization yields of helium resulting after the interaction with an ultrashort XUV pulse are obtained by numerically solving the full dimension time-dependent Schrödinger equation. The angular distributions reveal the underlying dominant mechanism, which depends on the effective photon energy absorbed and the pulse parameters. We specifically explore the contributions of radial and angular electron correlation terms. A single active electron picture is a qualitatively valid approach for the lowest photon energies, even in the above threshold ionization (ATI) region. Nonetheless, angular correlation plays a detectable role in the low energy region and a major role at higher energies when autoionizing states are populated. As the photon energy increases, sequential ionization-excitation dominates, therefore, the resulting probability distributions are explained as the result of two active uncorrelated electrons. This uncorrelated picture fails again for photon energies above ionization potential of the ion.

I. INTRODUCTION

Multiphoton ionization of atoms has received great attention since its experimental observation in the late sixties [1, 2]. The generation of pulsed lasers in the optical regime provided for the first time the necessary intensities for the observation of multiphoton transitions, not only between bound-bound, but also between bound and continuum states. It opened the way to two decades of active research to gain a deep understanding on the effects of resonances, coherence [3] and above threshold photon-absorption [4, 5] in the observed multiphoton ionization yields. The interest in multiphoton processes has undergone a resurgence in the current century with the advent of femtosecond and sub-femtosecond pulses in the UV/XUV and X-ray frequency domains and with the newly developed experimental techniques using reaction microscopes. Velocity correlation (VC) methods, velocity map imaging (VMI) or cold target recoil ion momentum spectroscopy (COLTRIMS) allow the detection in coincidence of the individual momenta of the charged fragments resulting after the ionization event. These experimental capabilities can now provide rich information on atomic and molecular ionization with unprecedented energy and time resolution. These tools thus give access to laser-induced coherences and ground-state and dynamical electron correlation in multiphoton ionization, and it is of fundamental interest to eventually manipulate the laser-induced electron dynamics in atoms and molecules. In the present work, we accurately evaluate the effect of electron correlation terms in a two-photon absorption process by analyzing the richest observable in atomic ionization, namely, the photoelectron angular distributions (PADs). The ionization probability distributions, differential in both energy and angle of the emitted electron, capture the multichannel character of the emitted fragments and are a direct signature of electron correlation [6].

The helium atom, the simplest multielectronic system, is the benchmark target par excellence to unravel the complexity of those phenomena. Two-photon single ionization of helium was subject of an extensive number of theoretical [7–10] and experimental [11–16] studies exploring total ionization yields, and more recently, photoelectron angular distributions (PADs) in the low energy region [17, 18]. However, to our knowledge, no previous investigations have provided a complete analysis on the expected angular distributions of electron emission upon the interaction with sub-fs pulses when above-threshold ionization (ATI) opens.

The angular distribution of the emitted electron is explained through the relative amplitudes and phases between the contributing partial waves at a given energy. However, it is interesting to understand how this observable captures the effect of the pulse duration, the electron correlation terms and the dominance of different bound-continuum and continuum-continuum transitions. In ref. [18], Ishikawa and Ueda already provided a thorough theoretical study on the pulse duration variation of the PADs on two-photon single ionization hydrogen and helium atoms, for photon energies below the first ionization potential, assuming pulses with durations in the range 1-21 fs. Their results were explained in terms of a single active electron process. In this work, we explore this process for photon energies up to 70 eV. We first show that this single active electron picture is qualitatively valid for photon energies below the ionization potential of the system, but breaks down as the energy increases a few eV. We then discuss the dominant mechanisms at larger

* alicia.palacios@uam.es

photon energies and examine the relevance of highly correlated mechanisms in two-photon single ionization of He.

We perform full *ab initio* calculations and propose a simplified model to elucidate the underlying mechanisms and the pulse dependencies of the total and energy and angle differential ionization yields after two-photon absorption by the helium atom. In particular, we discuss if the relevance of accounting for electron-electron interactions in both/either ground, intermediate and final highly excited states of the atom can be questioned [19, 20], in particular, when using two photons to excite the ground state of the atom ($He(1s^2)$) to autoionizing states such as those doubly excited states commonly denoted as $nln'l'(n, n' \geq 2)$. We explore the effect of accurately representing radial and angular electron correlation terms in both the ionization signal and the angular distribution of the ejected electron when ionizing with ultrashort pulses in the extreme ultraviolet (XUV).

II. METHODOLOGY

A. Time-dependent Schrödinger Equation

For an accurate evaluation of the two-photon single ionization of helium induced by ultrashort pulses, we solve the time-dependent Schrödinger equation (TDSE) in full dimensionality employing the methodology described in Refs. [21, 22]. We have extended the implementation to enable the extraction of the photoelectron angular distributions for the single ionization channel. The *ab initio* calculations are further rationalized in terms of simple analytical models. In the following, we review the most relevant theoretical details for the *ab initio* method. Expressions are given in atomic units unless otherwise specified. We assume that the He atom, initially in its ground state, is subjected to a time-varying pulse that starts at t_i and ends at t_f. To track the time evolution of the wave function, we solve the TDSE,

$$i\frac{\partial}{\partial t}\Psi(t) = \mathcal{H}(t)\Psi(t)\,. \tag{1}$$

with the full Hamiltonian, $\mathcal{H}(t) = H + V(t)$, which includes the interaction term of the atom with laser field, $V(t)$, and

$$H = T_1 + T_2 - \frac{1}{\mathbf{r}_1} - \frac{1}{\mathbf{r}_2} + \frac{1}{|\mathbf{r}_1 - \mathbf{r}_2|} \tag{2}$$

where the T_1 and T_2 are the kinetic energy terms, $T_i = -1/2\nabla_i^2$. The electron-electron interaction term is evaluated using the well-known multipole expansion in terms of spherical harmonics:

$$\frac{1}{|\mathbf{r}_1 - \mathbf{r}_2|} = \sum_{\lambda}\sum_{\mu=-\lambda}^{\mu=\lambda}\frac{4\pi}{2\lambda+1}Y_\lambda^{*\mu}(\hat{\mathbf{r}}_1)Y_\lambda^{\mu}(\hat{\mathbf{r}}_2)\frac{r_<^\lambda}{r_>^{\lambda+1}}\,. \tag{3}$$

The wave function is expanded in coupled spherical harmonics and using a radial discrete variable representation as described below in Sec. II D.

After the external field is turned off ($t > t_f$), the system evolves according to the time-independent Hamiltonian H of the isolated atom, $\Psi(t) = e^{-iH(t-t_f)}\Psi(t_f)$. We next define a scattered wave Ψ_{sc} by taking its Fourier transform from t_f to infinity,

$$\Psi_{sc} \equiv -ie^{-iEt_f}\int_{t_f}^{\infty} dt\, e^{i(E+i\epsilon)t}\,\Psi(t). \tag{4}$$

In the limit $\epsilon \to 0^+$, $\Psi_{sc} = G^+\Psi(t_f)$ [22], which is equivalent to solving,

$$(E - H)\Psi_{sc} = \Psi(t_f), \tag{5}$$

with pure outgoing boundary conditions [23]. Thus the scattered wave, from which we will extract all the physical information, satisfies a driven Schrödinger equation in which the propagated wavepacket at the end of the pulse appears as the source term. The numerical solution of Eq. (5) effectively propagates the wavepacket at the end of the laser pulse to $t \to \infty$ and Fourier transforms the result in a single computational step. One way to circumvent the explicit imposition of pure outgoing boundary conditions in the above equation is to use the Exterior Complex Scaling (ECS) method [21, 23]. In the ECS method, the electronic coordinates are (complex) scaled only beyond a given region ($r > R_0$) according to the transformation $r \to R_0 + (r - R_0)e^{i\eta}$. Once this transformation is applied, Ψ_{sc} may be obtained from Eq. (5) using a linear iterative solver implemented in PETSc libraries [24, 25] .

The explicit evaluation of the single ionization amplitudes $C(\mathbf{k}_n)$ is done in terms of the following surface integrals [23]:

$$\begin{aligned} C(\mathbf{k}_n) = \frac{1}{2}\int \big\{&\phi_{\mathbf{k}_n}^{-*}(\mathbf{r}_1)\phi_n^*(\mathbf{r}_2)\nabla\Psi_{\rm sc}(\mathbf{r}_1,\mathbf{r}_2) \\ &- \Psi_{\rm sc}(\mathbf{r}_1,\mathbf{r}_2)\nabla[\phi_{\mathbf{k}_n}^{-*}(\mathbf{r}_1)\phi_n^*(\mathbf{r}_2)]\big\}\cdot dS\,, \end{aligned} \tag{6}$$

where $\nabla = (\nabla_1, \nabla_2)$. The testing functions ϕ_n and $\phi_{\mathbf{k}_n}^-$ are given by the bound states of He^+ and the energy-normalized Coulomb functions with a nuclear charge $Z = 1$. The above expression allows us to extract the angular and energy dependent amplitudes, or equivalently ionization probabilities, for single ionization from the propagated wave packet.

B. Laser-atom interaction

We are interested in describing few-photon atomic ionization induced by finite laser pulses with wavelengths in the XUV, specifically in the 18.5-95 nm range. Therefore, the electric dipole approximation is valid and we can assume the electromagnetic field to be independent

of the spatial coordinates. The laser-atom interaction term $V(t)$, the time-dependent part of the Hamiltonian in Eq. (1), can thus be written as $V(t) = \mathbf{p}\cdot\mathbf{A}(t)$ in the velocity gauge or as $V(t) = \mathbf{r}\cdot\mathbf{E}(t)$ in the length gauge. The electric field $\mathbf{E}(t) = -\partial\mathbf{A}(t)/\partial t$, can be expressed as:

$$\mathbf{E}(t) = \begin{cases} E_0 f(t)\cos(\omega t)\hat{\boldsymbol{\epsilon}} & |t| < T/2 \\ 0 & \text{elsewhere,} \end{cases} \tag{7}$$

where $f(t)$ is an envelope that defines the finite duration of the pulse that we have chosen as $f(t) = \cos^2\left(\frac{\pi}{T}t\right)$. We restrict our investigation to linearly polarized light and to the interaction with pulses of moderate intensities in order to provide relatively large ionization rates for two photon transitions, but low enough to keep the processes within the weak field limit [21].

C. Two-photon single ionization cross sections

In the weak field limit, the second order time-dependent perturbation theory expressions apply and the ionization amplitudes for the two-photon transition from an initial state of energy E_i to a single electronic continuum final state of energy E_f can be written as

$$\begin{aligned} C^{2\omega}(\mathbf{k}_n) =& E_0^2 F^{2\omega}(E_f, E_m, E_i, \omega, T)\times \\ & \sum_m \langle\Phi_f^-|\hat{\boldsymbol{\epsilon}}\cdot\boldsymbol{\mu}|\Phi_m\rangle\langle\Phi_m|\hat{\boldsymbol{\epsilon}}\cdot\boldsymbol{\mu}|\Phi_i\rangle\,, \end{aligned} \tag{8}$$

where E_0 is the maximum field strength, $\hat{\boldsymbol{\epsilon}}$ is the unit vector defining the polarization direction of the field, $\boldsymbol{\mu}$ is the dipole operator in the length gauge, $T = t_f - t_i$ is the total pulse duration and the sum m is over all the eigenstates of the target. Considering a laser pulse as defined in Eq. (7), $F^{2\omega}(E_f, E_m, E_i, \omega, T)$ is the double integral in time given by

$$\begin{aligned} F^{2\omega}(E_f, E_m, E_i, \omega, T) =& \frac{1}{2}\int_{t_i}^{t_f} dt' e^{i(\Delta E_{fm}/\hbar-\omega)t'} f(t') \\ & \times \frac{1}{2}\int_{t_i}^{t'} dt'' e^{i(\Delta E_{mi}/\hbar-\omega)t''} f(t''), \end{aligned}$$

where $\Delta E_{ij} = E_i - E_j$. One can now connect Eq. (8) with the expression for the two-photon cross section by defining a "shape function" [21, 26]:

$$\begin{aligned} \widetilde{F}^{2\omega}(E_f, & E_m, E_i, \omega, T) = \\ & (E_i + \Delta E_{fi}/2 - E_m) F^{2\omega}(E_f, E_m, E_i, \omega, T). \end{aligned} \tag{9}$$

As we explained in Refs. [21, 22], if the photon frequency ω is not too close to being in resonance with a transition to one of the intermediate states Φ_m, then the shape function $\widetilde{F}^{2\omega}$ is well approximated by an expression that does not depend on the energies of the intermediate states in the sum in Eq. (8) and which becomes exact in the long T limit. For the pulses as defined in Eq. 7, the shape function may be written as,

$$\begin{aligned} \widetilde{F}^{2\omega}(E_f, E_m, E_i, & \omega, T) \approx \widetilde{\mathfrak{F}}(E_f, E_i, \omega, T) \\ & = \frac{12\sin\left(\frac{\xi T}{2}\right)\pi^4}{\xi\left[T^4\xi^4 - 20\pi^2T^2\xi^2 + 64\pi^4\right]}\,, \end{aligned} \tag{10}$$

where $\xi = (2\omega - \Delta E_{fi})$ is the generalized detuning parameter. In order to compare the total ionization yields for different pulse durations and with previous data obtained in the limit of infinitely long pulses, the two-photon single ionization cross section can be then written as:

$$\frac{d\sigma^{2\omega}}{d\Omega} = \frac{(2\pi)^3\hbar^3 k_n \alpha^2}{(\Delta E_{fi}/2)^2 m^3}\frac{|C(\mathbf{k}_n)|^2}{E_0^2|\widetilde{\mathfrak{F}}(E_f, E_i, \omega, T)|^2} \tag{11}$$

The above expression allows one to extract the cross sections differential in both angle and energy of the emitted electrons from a time-propagated wave packet for the whole range of photon energies within the bandwidth of the pulse [27]. It is worth to highlight that $C(\mathbf{k}_n)$ as defined in Eq. (6) are the physical amplitudes for a given pulse, i.e. these are strictly exact in the current formalism and, therefore, there also the corresponding angular differential ionization probabilities given by $|C(\mathbf{k}_n)|^2$. In other words, the angular distributions retrieved through the present methodology are those that would be experimentally measured. We have only introduced an approximation through the "shape function" in Eq. 10 in order to provide an expression for the cross sections, Eq. (11), which affects the magnitude resulting for the total ionization cross section (allowing direct comparisons of results for different pulse durations), but only implying a scale factor for the electron angular distributions.

D. Computational details

Assuming the helium atom in its ground state (^{1}S^e), only channels with total symmetry ^{1}S^e, ^{1}P^o and ^{1}D^e (L = 0, 1 and 2) are accessible through one and two-photon absorption processes following the optical selection rules. The two-electron wave function is expanded in terms of products of coupled spherical harmonics to represent the angular components and the radial degrees of freedom are discretized using a finite-element, discrete variable representation (FEM-DVR) with a product basis of Lobatto shape-functions [28]. We include all (L, l_1, l_2) possible configurations for given maximum values of l and L. Because the present work is performed within the weak-field limit, convergence for second order processes from the ground state ($L = 0$) is achieved with $L_{max} = 2$. The smallest value required for the expansion in angular momenta in $l_{1,2}$ will depend on the photon energies employed. We found that for the range of energies considered, numerical convergence is achieved with $l_{max} = 5$.

The ground-state wave function, Ψ_0, is obtained by diagonalizing the field-free Hamiltonian H on a real grid ($r_{max} \approx 50$ Bohr). The absolute value for the ground state energy obtained is -2.9036 au, differing from previous accurate extrapolated Hylleraas-type calculations [29] in 10^{-4} au. The time-dependent wavepacket is then propagated in the presence of the external field within the length gauge according to Eq. (1), over the duration of the pulse, in a larger region of space, including $r_{max} = 200$ a.u. The propagation is carried out numerically using the Crank-Nicolson method, with a time step $\Delta t = 4 \times 10^{-3}$ atomic units.

III. ANGULARLY-RESOLVED IONIZATION PROBABILITIES

We employ a 2-fs pulse with a laser intensity of 10^{12} W/cm^2 to ionize helium by two-photon absorption. A diagram with the energetics is provided in Fig. 1. The total and fully differential probabilities are examined here for photon energies up to ~ 70 eV. Fig. 2 shows the total

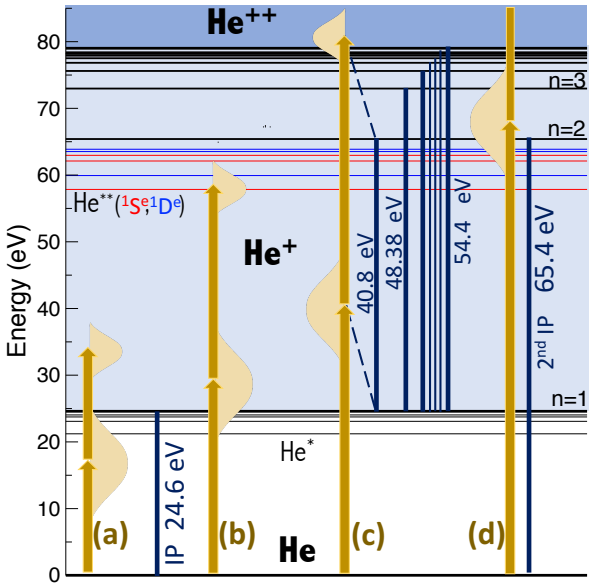

Figure 1. Schematic representation of the relevant transitions for two-photon single ionization of helium. We indicate four regions discussed in the text leading to two-photon single ionization with photon energies: (a) below the single ionization threshold, 24.6 eV, (b) above threshold ionization where the two-photon absorption reaches the doubly excited states ($\omega > 28.95$ eV), (c) two-photon single ionization where core-excited resonances dominate and (d) region where the simultaneous excitation-ionization is energetically open already for one-photon absorption.

and partial cross sections as a function of energy, together with the photoelectron angular distributions obtained for a few specific energies. In order to minimize the importance of purely spectral effects in the resulting photoelectron distribution, i.e., those associated to the large frequency bandwidth of the ultrashort pulse employed, we extract the angular differential observables for a specific final energy. Because a two-photon transition from the ground state of helium reaches the continuum states of ^{1}S^e and ^{1}D^e symmetries, we have included the partial cross sections (red line with circles for ^{1}S^e and blue line with squares for ^{1}D^e) together with the total cross section (black thick line) as a function of photon energy. As expected by Fano's propensity rule [30], the contribution of the ^{1}D^e states is larger (by a factor ≥ 2) than the ^{1}S^e contribution. The only exception appears when a doubly excited state of ^{1}S^e symmetry is populated and direct ionization and autoionization interfere leading to the well-known Fano profile [31]. Although the relative contributions of ^{1}S^e and ^{1}D^e symmetries hardly varies along the whole range of photon energies, we do observe that the photoelectron angular distributions appreciably change with the photon energy.

For the lowest photon energies (< 29 eV), a simple single-active electron picture is able to provide a reliable description of the two-photon process. Mostly second order paths such that, He(1s^2) $\xrightarrow{\omega}$ He*(1snp) $\xrightarrow{\omega}$ He$^+$(1s) + e$^-$(ks+kd), contribute to the ionization yields. The atom is first promoted to an intermediate (bound or continuum) state represented by a 1snp or 1skp configuration, followed by the absorption of the second photon. This leaves the system in a final state with one bound electron in the He$^+$(1s) state, where the already excited electron was further promoted to the continuum in a s or d partial wave with energy $E_f = 2\omega - I_p$. Consequently, the resulting angular distributions can be easily rationalized in terms of the coherent superposition of ionization amplitudes with two main angular components, those associated to individual uncoupled spherical harmonics Y_{00} (S) and Y_{20} (D) [12, 17, 18]. The PADs can then be reduced to:

$$I(\theta) \propto |\mathcal{F}^S Y_{00} + \mathcal{F}^D Y_{20}|^2 \qquad (12)$$

where $\mathcal{F}^S$ and $\mathcal{F}^D$ are the complex amplitudes for the ^{1}S^e and ^{1}D^e symmetries at a given photoelectron energy. In Refs. [17, 18], the energy range between $\omega = 19$ eV to 25 eV was examined, explaining how the relative contribution of the resonant term (those singly excited states whose transition frequency lies within the pulse bandwidth) and the non-resonant term (resulting from the sum over all *virtual* intermediate states) reflects in both the total ionization yields and the photoelectron angular distributions for different pulse lengths [18].

The first two PADs in Fig. 2, at 15 and 18 eV, show a characteristic d shape (Y_{20} alone), since the D contribution to the total cross section is at least five times larger than that of S symmetry. Moreover, at these energies, the non-resonant term, which is nearly independent of the pulse duration, dominates, the PADs thus remain mostly unchanged when increasing the pulse duration [18]. However, for photon energies resonant (within the bandwidth of the pulse) with the $1snp\,^1P$ bound excited states, between 21.2 and 24.6 eV, both the resonant and

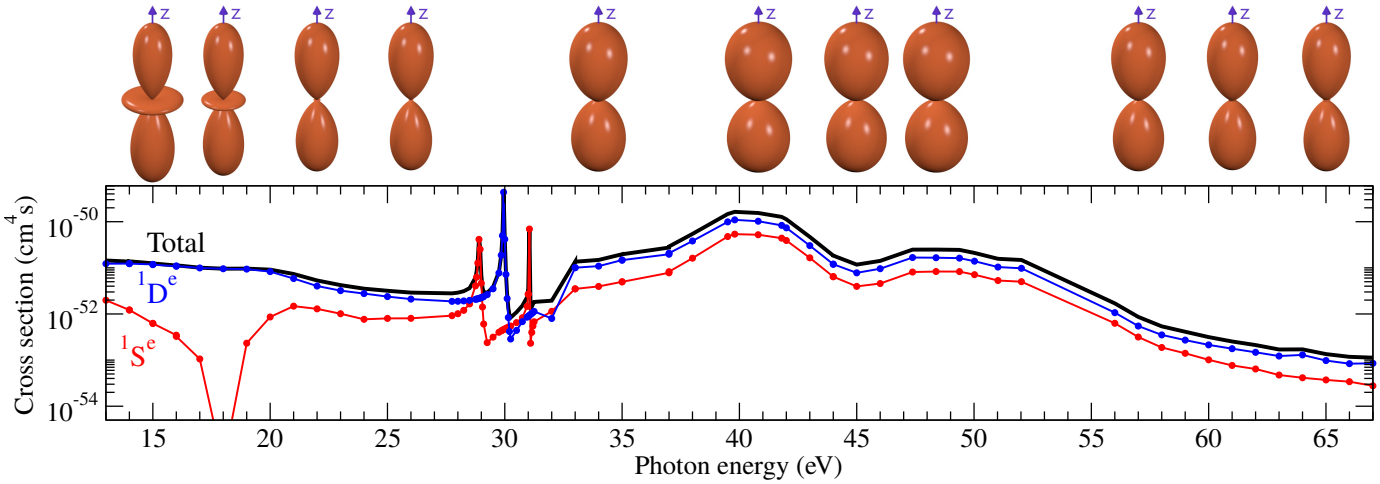

Figure 2. Total cross sections for two-photon single ionization of helium using a 2-fs pulse as a function of the photon energy absorbed. Black thick full line: total ionization yield. Blue with dots: D contribution. Red with dots: S contribution. The photoelectron angular distributions corresponding to a given energy of the emitted electron are plotted as insets. Distributions are plotted for effective photon energies of 15, 18, 22, 26, 34, 40.8, 45, 48.38, 57, 61 and 65 eV.

non-resonant paths significantly contribute. The dependence on pulse duration is already clearly captured in the total yields, as shown in figure 3. In this figure, we compare our TDSE results obtained for pulse durations of 2, 3 and 4.2 fs. We also include existing theoretical data obtained for infinitely long pulses using time-independent perturbation theory approaches [9, 32–34]. There is a noticeable pulse-length dependence around the photon energies in resonance with the singly excited states of the atom, which will also be reflected in the angular distributions as discussed in [17, 18]. This is the case for the PAD corresponding to $\omega = 22$ eV, lying near the excitation energy of the $1s2p\,^1P$ state (21.2 eV), where electron ejection in the plane perpendicular to the light was found to increase with the duration of the pulse and vanish for short pulse duration [18]. For the 2-fs pulse, it can further observed in Fig. 2 that, indeed, the PAD resembles that obtained at $\omega = 26$ eV, approximately one eV above the threshold of the ATI region where the angular distributions again hardly vary with pulse duration. The clear resemblance between these two is due to the contribution of the continuum-continuum couplings, which dominates the two-photon processes, even at 22 eV, also favored by the wide energy bandwidth of the pulse ($\Delta\omega \sim 2$ eV). The largest contribution of the ATI couplings at these energies have been confirmed with an analytical model that is introduced in section IV.

The PADs are significantly different from those at lower energies for an effective absorption of two photons of 34, 41, 45 and 49 eV. Although there is not a significant difference in the relative contribution of the S and D amplitudes with respect to the lower energy range, these distributions present an almost pure cosine-squared shape, with strictly zero probability of emission in the plane perpendicular to the polarization direction. These distributions are the signature of ionization of a bound $l = 0$ electron into the p-wave continuum. In this region, excitation sequentially follows ionization: the first photon absorption ejects one electron at an energy ($E_e = \omega - I_p$) and the second photon excites the ion. Due to the large oscillator strength associated with the excitation of the parent ion, as compared to a continuum-continuum transition, this contribution becomes the dominant as soon as it is energetically allowed. The longer the pulse the sharper the peaked structure in the total yield [21], as is also clear from Fig. 3 when infinitely long pulses are employed. The total cross section exhibits a monotonic increase that

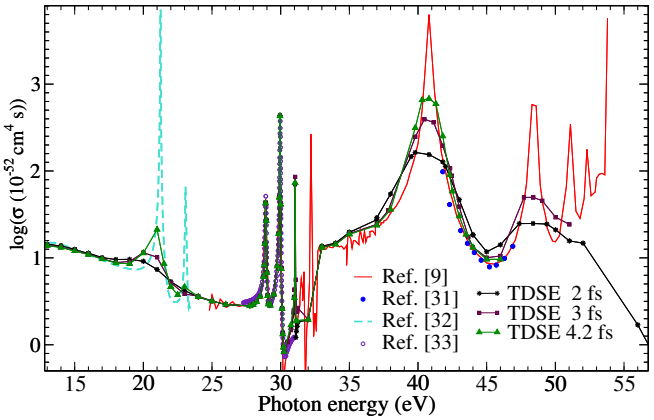

Figure 3. Two-photon single ionization cross section of helium as a function of the photon energy absorbed. Comparison with previous works using time-independent perturbation theory approaches. Full red line: ref. [9]. Blue filled dots: ref. [34]. Turquoise dashed line: ref. [33]. Brown circles: ref. [32]. Full lines with symbols: Apparent cross sections resulting after solving the TDSE for a pulses with a laser intensity of 10^{12} W/cm^2 and durations of 2 fs (stars), 3 fs (squares) and 4.2 fs (triangles), as indicated in the legend.

reaches a maximum at 40.8 eV, coinciding with the first excitation energy of the ion, $He^+(n=2)$–$He^+(n=1)$ [9, 35]. Additionally, a second local maximum is observed for $\omega = 48.38$ eV, in coincidence with the second excitation energy of He^+ from $n=1$ to $n=3$. These sequential ionization-resonant excitation have also been called "core-excited" resonances in refs. [9, 35], although it should be pointed out that this terminology is largely unrelated to the widely known core-excited autoionizing states for multielectronic targets. These core-excited resonances are intermediate-state resonances, where the photon energy is resonant with the transition from the ground state of the ionized species to an excited state, therefore the resulting total ionization probabilities upon two-photon absorption again depend on the pulse duration in this energy range as clearly captured in Fig. 3. This figure also show that the two-photon cross sections decrease for photon energies above 50 eV. In contrast with the results of the perturbative approach employed in ref. [9], whose validity is questionable as core-excited resonances accumulate, higher excitations are accurately accounted for in our calculations. A 2-fs pulse only resolves the resonant structures of the first two excited states, just because the pulse bandwidth is larger than the energy spacing between the subsequent peaks. The dominance of these *sequential* ionization-excitation mechanisms already implies that a single active electron picture, as shown in Eq. (12), cannot explain the observed PADs. Instead, the angular configurations associated to the Y_{10} spherical harmonic for a photoelectron leaving the helium ion in the resonantly excited $He^+(np)$ states dominate. One thus observes a behavior of two active mostly uncorrelated electrons, i.e. $He(1s^2) \xrightarrow{\omega} He^+(1s) + e^-(kp) \xrightarrow{\omega} He^+(np) + e^-(kp)$, and the resulting PADs are equivalent to those of a one-photon absorption from an s orbital.

For photon energies above $\simeq 54.4$ eV (ionization potential for the He^+), core-excited resonances no longer dominate. The angular distributions become more narrowly focussed along the polarization direction and the electron emission in the plane perpendicular to the polarization is again allowed, even though hardly visible in Fig. 2. This relatively subtle effect can be better seen in the figure provided in the appendix A. At 65.41 eV, a one-photon transition can reach the n=2 ionization threshold of He^+, i.e. one photon absorption can directly eject one electron into the continuum and simultaneously excite the second electron into the He^+(n=2), which can only be achieved by explicitly accounting for the electron correlation.

IV. BETA PARAMETERS ANALYSIS

A more quantitative analysis for the photoelectron angular distributions can be accomplished by defining the asymmetry parameters β_j to express the angle- and energy differential cross section as:

$$\frac{d\sigma^{2\omega}}{d\Omega} = \frac{\sigma(\omega)}{4\pi} \sum_j^{2N} \beta_j(\omega) P_j(\cos\theta), \tag{13}$$

where σ is the total cross section, N is the number of absorbed photons, $P_j(x)$ is the Legendre Polynomial of order j, θ is measured with respect to the polarization direction of the radiation. The β_j parameters are obtained from the angular and energy differential ionization amplitudes (Eq. 6) and are given by [36],

$$\beta_j = \frac{1}{\sigma} \sum_{n,l} \sum_{\substack{L,l_k \\ L',l'_k}} (-1)^{j-L-L'-l} (2j+1) \sqrt{(2l'_k+1)(2l_k+1)(2L+1)(2L'+1)} \begin{pmatrix} l_k & l'_k & j \\ 0 & 0 & 0 \end{pmatrix} \begin{pmatrix} j & L & L' \\ 0 & 0 & 0 \end{pmatrix} \begin{Bmatrix} j & l_k & l'_k \\ l & L' & L \end{Bmatrix} \left[(-i)^{l'_k} e^{i\eta_{l'_k}} \mathcal{F}^{L'}_{l'_k,l}(n) \right]^* \left[(-i)^{l_k} e^{i\eta_{l_k}} \mathcal{F}^{L}_{l_k,l}(n) \right] \tag{14}$$

where $\mathcal{F}^L_{l_k,l}(n)$ are the radial matrix elements for the ejection of an electron with momentum k and leaving the remaining ion in the n,l state [37], which are connected to the amplitude expression given in Eq. 6 as:

$$C(\mathbf{k}_n) = \sqrt{\frac{2}{\pi}} \sum_{L,l_k,m_k} (-i)^{l_k} e^{i\eta_{l_k}} (l_k m_k l m | L0) Y^{m_k}_{l_k}(\hat{\mathbf{k}}) \mathcal{F}^L_{l_k,l}, \tag{15}$$

where $(l_k m_k l m|L0)$ are the Clebsch-Gordan coefficients. In a second order process, where only S ($L=0$) and D ($L=2$) components contribute, Eq. (13) is given just by a combination of β_2 and β_4, besides the trivial $\beta_0 = 1$.

Additionally, since the second ionization threshold of helium [$He^+(n=2)$–$He(1s^2)$] is 65.41 eV (see Fig. 1), for photon energies up to 32.7 eV the He^+ ion left behind can only occupy its $1s$ ground state. Consequently, the resulting distributions can be obtained just through a coherent sum of two amplitudes, as in Eq. (12). In this case, the asymmetry parameters in Eq. (14) can be

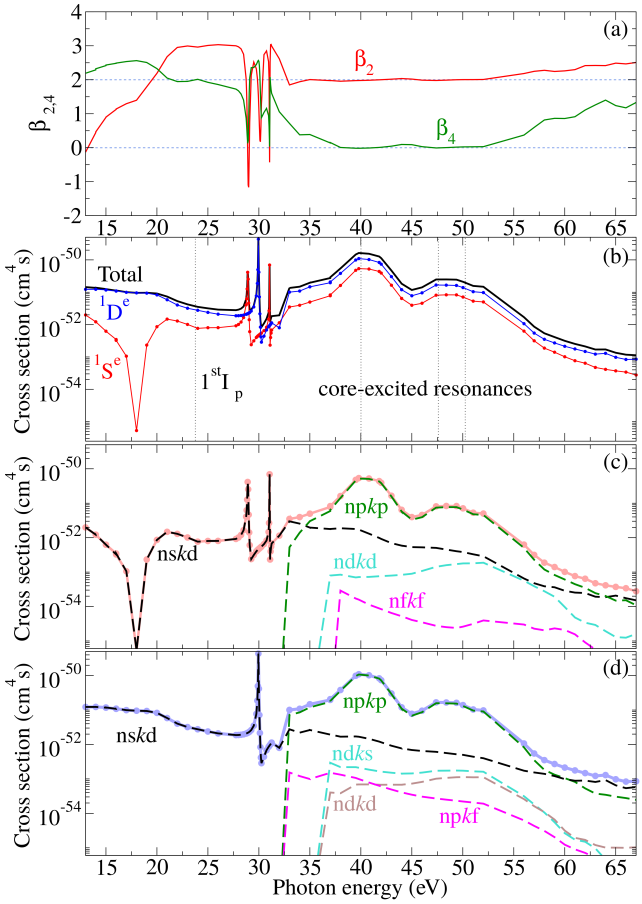

Figure 4. (a) Asymmetry parameters, β_2 and β_4, as a function of photon energy. (b) Corresponding total and partial (S and D) cross sections for the two-photon single ionization using a 2-fs pulse. Dotted vertical lines indicate the energy of the ionization potential for helium ($I_p = 24.6$ eV) and the excitation energies for the ion from He^+(1s) to He^+(n=2), He^+(n=3) and He^+(n=4). (c) Contribution of the different ionization channels with one electron in the remaining ion, He^+(ns, np, nd, etc), and the emitted electron with a particular angular momentum (ks,kp,kd,...) for a total final S symmetry. (d) Same as (c), contributions from different ionization channels for a total final symmetry D.

simplified to the expressions [12, 17, 18]:

$$\beta_2 = \frac{10}{W^2+1}\left[\frac{1}{7} - \frac{W}{\sqrt{5}}\cos\delta\right] \quad (16)$$

$$\beta_4 = \frac{18}{7(W^2+1)} \quad (17)$$

where $W = |\mathcal{F}^0_{0,0}|/|\mathcal{F}^2_{2,0}|$ and $\delta = \arg\left(e^{i\eta_0}\mathcal{F}^0_{0,0}/e^{i\eta_2}\mathcal{F}^2_{2,0}\right)$, i.e., W accounts for the relative absolute value of the amplitudes for S and D contributions, while δ is their relative phase. These expressions allow us to obtain two limiting cases, according to the dominant S or D contribution, that will be useful later in this section. Firstly, if the D contribution is much larger than the S one, ($|\mathcal{F}^0_{0,0}| \ll |\mathcal{F}^2_{2,0}|$), then $W \sim 0$ and the asymmetry parameters will be given by $\beta_2 \sim 10/7$ and $\beta_4 \sim 18/7$. On the other hand, if the S contribution to the total cross section is much larger than the D one, then $W \gg 1$ and the asymmetry parameters will be given by $\beta_2 \sim -\sqrt{20}\cos\delta/W$ and $\beta_4 \sim 0$.

In Fig. 4(a), we show the asymmetry parameters $\beta_{2,4}$ for the entire energy range under investigation. For completeness, we have also included the total cross sections in panel (b), as well as the partial cross sections identifying the contribution from different ionization channels (leaving He^+ in an ns state, or in a np state,...) to final states of S (panel c) and D (panel d) symmetries. In the lowest-energy region, and up to $\omega = I_p = 24.6$ eV, the β_2 value increases while β_4 decreases with photon energy, reaching a plateau between $\sim 24-29$ eV. The significant change in $\beta_{2,4}$ observed up to 24.6 eV is mostly the result of the larger contribution of the "virtual" transitions involving the continuum-continuum couplings when using significantly short pulses. We have confirmed this behaviour using the semi-analytical model described below [38]. The same dominance of the virtual ATI transitions in this energy region was also found in two-photon single ionization of H atom, right below the ionization threshold.

In the limit for infinitely long pulses, the radial matrix element $\mathcal{F}^{S(D)}$ presents a minimum value before (after) each maximum corresponding to the resonant singly excited states of helium [8, 33]. Consequently, the $\beta_{2,4}$ values will alternate between those corresponding to the limiting cases $W \gg 1$ and $W \sim 0$, the latter being independent of the phase difference δ. For a 2-fs long pulse, we can only resolve the first minimum in the S contribution of this sequence, however longer pulses are able to resolve more of these structures [18, 22]. In Figure 5, we plot the β_2 and β_4 values resulting from solving the TDSE with the 2-fs pulse (black thick line). We also include the results from reference [18], where they used pulses of $T_{1/2} = 7$ fs duration at full width half maximum (FWHM, $T_{1/2} = 2\sqrt{\ln 2}\,T$) (black thin line), corresponding to a duration of $T = 4.2$ fs. The energy bandwidth of a 4.2 fs pulse is narrow enough to resolve in energy the resonant contributions of the first two $1snp$ singly excited states of the atom. The resonant contribution thus gain importance at these specific energies, strongly modifying the PADs [18]. In order to show that a single-active electron approach remains valid to describe the two-photon ionization yields, and more importantly, the PADs, even for photon energies where above-threshold ionization is accessible, we have used an analytical model based on second order time-dependent perturbation theory.

We have evaluated the time-dependent perturbation theory expression (Eq. (8)), using a semi-analytical approximation [38] as it follows. We approximate the helium ground state by a $1s$ hydrogenic orbital, with effective charge $Z_{eff} = \sqrt{-E_{He}} \sim 1.704$, allowing us to recover the fully converged ground state energy. This effective charge is close to the value obtained from a textbook variational calculation using a single $1s$ orbital,

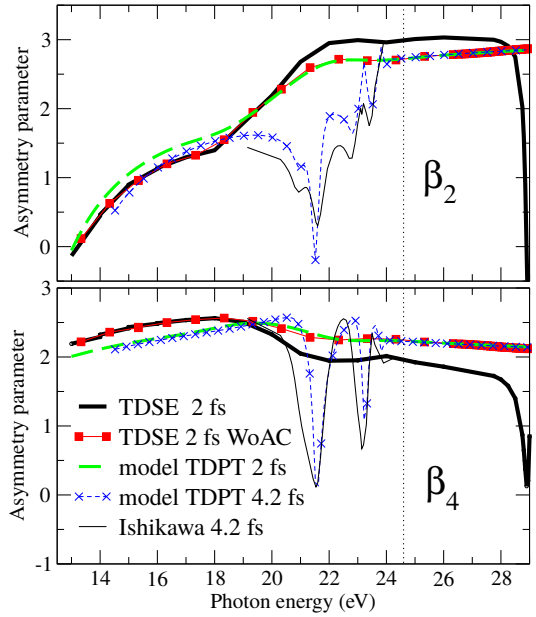

Figure 5. Asymmetry parameters, β_2 (upper panel) and β_4 (bottom panel) as a function of the photon energy. Comparison with the β parameters resulting from the *ab initio* simulation (TDSE 2 fs) and a *truncated* calculation removing the angular correlation terms (TDSE 2 fs WoAC), both employing a 2-fs pulse. We also include the results of a single-active electron model based on TDPT (see main text) using a 2-fs (model TDPT 2 fs) and a 4.2 fs pulse (model TDPT 4.2 fs), and the results by Ishikawa and Ueda [18] reported for a 7 fs pulse duration at FWHM, equivalent to T=4.2 fs.

and it is nearly coincident with effective charge from the Slater rules. The intermediate (bound excited and single continuum) states are approximated by hydrogenic orbitals with $Z = 1$ for the excited/outgoing electron. In this way, electron repulsion is approximately taken into account by a full shielding of the outer electron by the inner one ($r_{12}^{-1} \simeq r_{outer}^{-1}$) without explicitly accounting for electron correlation terms. We retrieve the β parameters with the model assuming a 2-fs (green dashed line) and a 4.2-fs pulse (dashed line with crosses), plotted in figure 5. The model presents a very good agreement with the outcome of the *ab initio* calculations for $\beta_{2,4}$ up to $\omega \sim 29$ eV, although slightly underestimates/overestimates the value for β_4 for photon energies below/above the ATI-like region.

In order to attain a deeper understanding of this effect, we further perform a *truncated ab initio* simulation, where we solve the TDSE removing the angularly correlated electronic terms in the Hamiltonian, therefore neglecting those terms involving electrons with different angular momenta (i.e., Eq. 3 is reduced to $\lambda = 0$). The results of the *truncated ab initio* simulation are also shown in Fig. 5 (red line with squares). The remarkably good agreement between the truncated simulation and the model confirms that the slight deviations of the simple analytical model with respect to the full numerical simulations are mostly due to the angular correlation term. Indeed, the results of the model and the *truncated ab initio* results are almost indistinguishable above 22 eV, thus confirming that approximating r_{12}^{-1} by r_{outer}^{-1} incorporates most of the relevant radial electron-electron interaction in this photon energy region. In other words, that the angular and energy dependencies of the process can be accounted through the transitions 1s1s $\rightarrow$ 1snp(kp) $\rightarrow$ 1s ks,kd, where 1s are the natural orbitals minimizing the ground state energy. The crossing of the $\beta_{2,4}$ parameters observed at $\omega \sim 20$ eV in Fig. 4 corresponds to a near ATI threshold behavior (in the limit $T \rightarrow \infty$) which is shifted to smaller photon frequencies due to the pulse bandwidth ($\Delta\omega \sim 2$ eV). This feature is of general character for atomic targets as checked performing second order Time-Dependent Perturbation Theory calculations for H atom. On the other hand, the plateau is nearly independent of the pulse duration T and originates from the apparent validity in this case of Fano's propensity rule with $W \sim 0.5$ and $\delta \sim \pi$ [17] leading to $\beta_2 \sim 2.93$ and $\beta_4 \sim 2.06$, in very good agreement with results obtained in that energy region.

For $\omega > 32.7$ eV, the probability of populating $n > 1$ states of the residual ion upon two-photon absorption starts to rise. For photon energies up to 50 eV the dominant contribution to the $^1S^e$ and $^1D^e$ final states is given by the $np\epsilon p$ configurations, as can be seen in Fig. 4 (c) and (d). This corresponds to a picture of two active (mostly) uncorrelated electrons, leaving the helium ion in a np state. Additionally, in this scenario, the full expression for the asymmetry parameters in Eq. (14) can be simplified to $\beta_2 \sim 2$ and $\beta_4 \sim 0$, revealing thus the uncorrelated character of the two-photon transition in this energy region.

For photon energies above 50 eV, several configurations (ns$k$s, np$k$p, nd$k$s, nd$k$d, etc) contribute to the cross sections and the single configuration approximation is no longer valid. It can be seen in Fig. 4 (b) and (c) that the probabilities of leaving the residual ion in ns$k$d and np$k$p D states and in ns$k$s and np$k$p for S states are similar, which is captured in the trends observed for the β parameters.

V. ELECTRON CORRELATION IN AUTOIONIZING PROCESSES REACHED BY TWO-PHOTON ABSORPTION

The more pronounced variation of the β parameters with photon energy occurs in the energy range where the series of autoionizing states are reached. This is a consequence of the predicted variation of the relative values of S and D amplitudes along the Fano profiles. The trends observed for the photoelectron emission close to this series of autoionizing states, are indeed independent of the pulse duration as it was shown in Fig. 3. Note that, in contrast with intermediate resonances that are populated in the one photon transition and, consequently, short

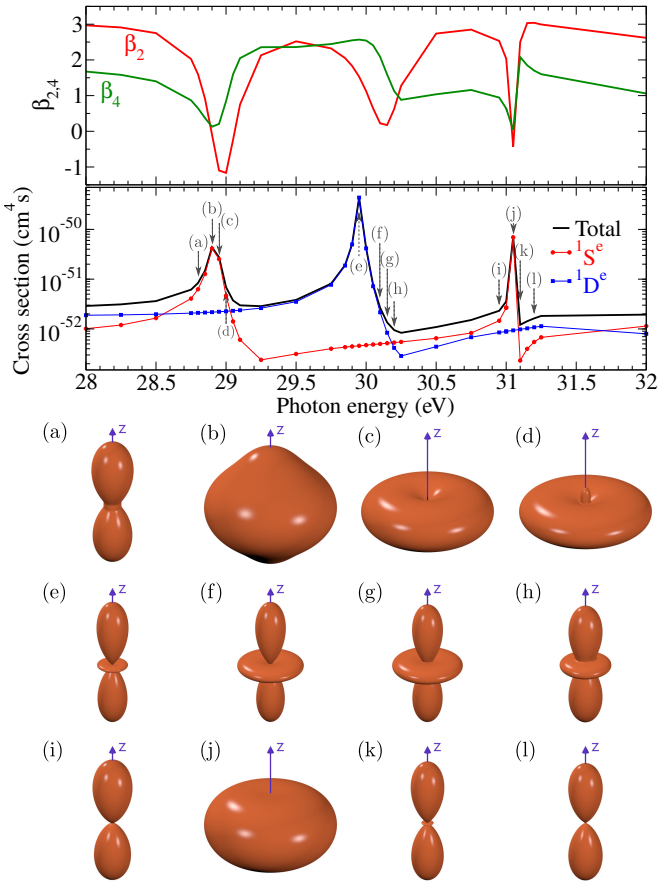

Figure 6. As in Fig. 4(a) and (b), β parameters and cross sections zoomed in the energy region where the doubly excited states are populated upon two-photon absorption. The vertical dotted lines indicate the energies at which the photoelectron angular distributions plotted in the bottom of the figure are computed, as accordingly label. The first row of PADs correspond to the first $^1S^e$ doubly excited state $(_2(1,0)_2^+$ or 2s2s). The second row corresponds to the first $^1D^e$ doubly excited state $(_2(1,0)_2^+$ or 2p2p). And the third row corresponds to the second $^1S^e$ doubly excited state $(_2(-1,0)_2^+$ or 2p2p).

pulse durations smooth out their peaked structures, the doubly excited states are final states. These are reached after a two-photon absorption, therefore, as long as the photoelectron energy is measured with enough resolution their sharp Fano profiles will be revealed independently of the pulse duration employed in the interaction. Figure 6 is an enlargement of panels (a) and (b) of Fig. 4 in this region. We have also included the PADs at specific energies around each of the autoionization peaks shown. The PADs corresponding to the maxima ionization probability associated to $^1S^e$ doubly excited state, (b) and (j), present a nearly spherical distribution compatible with an almost pure outgoing s-wave, distributions that mostly ignore the electromagnetic field direction. Upon population of the metastable highly excited state, the system decays into the $1sks$ electronic continua due to electron correlation, with an almost zero value of β_4, evidently losing memory of the initial light-induced transition.

The almost spherical shape at the Fano peak resulting from the autoionization decay of the first $^1S^e$ metastable state can be easily understood from equations (16) and (17). Since $W >> 1$, we expect $\beta_2 \simeq -\sqrt{20}\cos\delta/W$ and $\beta_4 \simeq 0$. Moreover, as W reaches its largest value, $\beta_2 \to 0$, resulting in an isotropic distribution. In the inset figures (a) to (d), we see the evolution of the PAD along the Fano profile of the lowest $^1S^e$ doubly excited state, where the phase of the amplitude associated to a given channel undergoes a change of π which results in a rapid evolution of the PAD from almost spherical in (b) to a mostly perpendicular ejection of the electron in (c), to a combination of both in (a) and (d). A comparable evolution is also found for the PADs across the second autoionizing state of $^1S^e$ symmetry, panels (i) to (l), where the interference between both waves leads to a negligible probability of photoelectron ejection in the perpendicular plane in (i) to an almost spherical distribution in (j). In contrast, around the excited state of D symmetry the changes are apparently less pronounced due to the strong dominance of the d-wave. These angular distributions can be easily explained, taking into account that the available energy only allows to populate the $1s$ ground state of the remaining ion. Therefore, upon decaying the only degree of freedom available is the angular momentum of the ejected photoelectron, which is adjusted to satisfy the selection rules. Angular correlation is thus mandatory for the description of these features and the rapid changes in energy of the PADs is revealing this strong correlated character of the final state.

Ionization by two photons would seem to allow processes like ionization of the $1s^2$ ground state of helium via autoionizing states nominally identified as $2p2p$, or with a strong contribution of such configurations, to proceed largely via the uncorrelated absorption of two separate photons and to be described without appealing to electron correlation. Two-photon ionization through autoionizing states is not so simple however. In order to expose the role of electron correlation in both the initial and final states in this process, as well as at photon energies where autoionization does not occur, we have performed two tests in which we eliminate various correlation contributions in order to identify their roles.

Firstly, we perform a S-Wave single-active-electron (SW-SAE) approximation, where (i) we assume an $S-wave$ approximation for the ground state (only configurations of the type $(L, l_1, l_2) = (0, 0, 0)$ are included, conventionally called the "radial limit" for two-electron bound states) and, (ii) restrict the transition to a single active electron approximation, *i.e.*, forcing one of the electron to remain in its initial ns configuration. Such a restriction implies that the configuration space will include the following set of angular configurations: $(L, l_1, l_2) = (0, 0, 0), (0, 1, 0), (0, 0, 1), (2, 2, 0), (2, 0, 2)$.

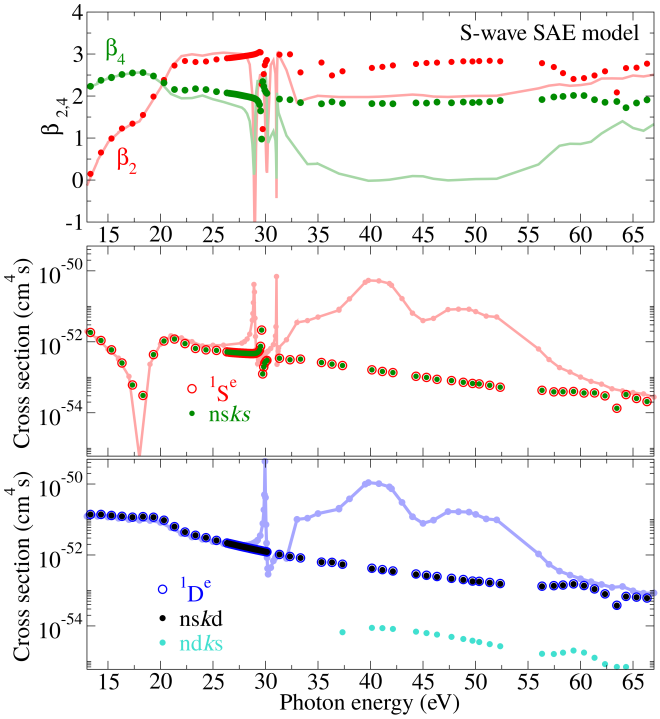

Figure 7. β parameters (upper panel) and total cross sections for two-photon single ionization into $^1S^e$ (middle panel) and $^1D^e$ (bottom panel) final symmetry using the S-wave "single-active electron" approximation described in the text. Contributions form each ionization channels are also included. The ground state of helium is retrieved within the S-wave approximation using an $l_{max} = 0$, and the subsequent electronic transitions are only allowed within a single active electron approach. Note nevertheless that all electron correlation terms within the S-wave SAE approximation are accounted for.

Note that the electron interaction term $1/r_{12}$ is fully included within this active space. The results of the SW-SAE approximation are plotted in dotted lines in Fig. 7. We show the β-parameters in the upper panel, and the $^1S^e$ and $^1D^e$ partial contributions in the middle and bottom panels, respectively. For a meaningful comparison with the full *ab initio* simulations (faint colored full lines in the figures), we have shifted our results accounting for the energy shift obtained for the ground state because of the use of the $S-wave$ approximation. As explained in section III, both the total ionization yields and the β parameters are expected to be reasonably described by the single-active-electron picture for photon energies below the first ionization threshold of helium, and even in the low ATI region. As soon as the doubly excited states are reached, this approximation completely breaks down, since in this model only one of the electrons is allowed to change its angular momentum. Even if the total Hamiltonian contains all radial and angular electron correlation terms for the active space chosen, the signature of doubly excited states for the $^1D^e$ symmetry has completely vanished in this approximation. The reason is the absence of the main configurations describing the doubly excited states in the *active space*, i.e. the *npnp* ones. Although the final configuration with the largest weight in the region where the $^1D^e$ doubly excited states appear is accounted for (*nskd*), and the corresponding electron correlation terms are included, we are including only the direct photoionization term and fully prevented autoionization. We have removed the possibility of each electron separately absorbing a photon and the correlation terms associated to them. Interestingly, the profile for the first $^1S^e$ doubly excited state still appears, although significantly reduced by the lack of the *npnp* and *ndnd* configurations, but it is still visible, therefore revealing a strong *nsns* character of the doubly excited states of $^1S^e$ symmetry in contrast with the $^1D^e$ autoionizing states series. Above $\sim$ 32 eV, the SW-SAE model expectedly fails, since two-active electron mechanisms dominate as already discussed.

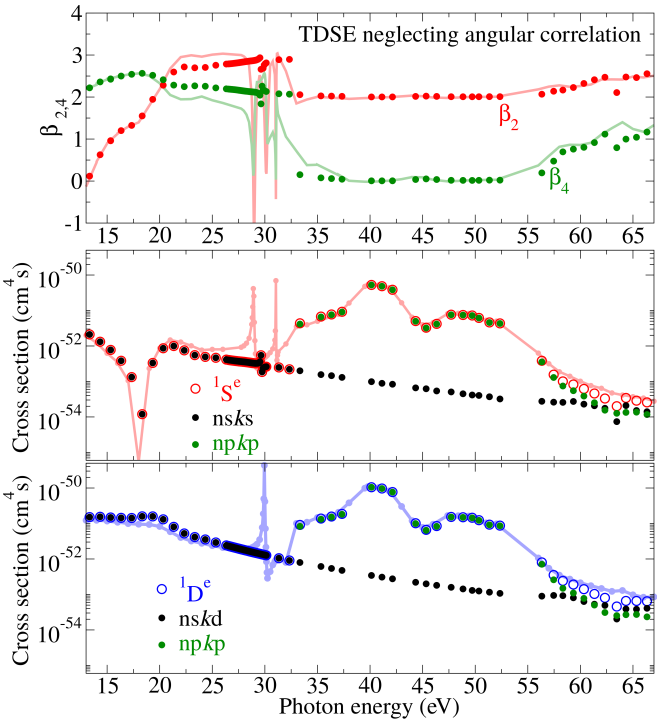

Figure 8. Same as Fig. 7, but for a truncated simulation without angular correlation (WoAC), i.e. solving the TDSE in full dimensionality where the angular correlation terms are neglected.

We have thus perform a different truncation in the Hamiltonian, where now both electrons are active, we assume a complete basis set, but the angular electron correlation term is fully suppressed and the calculation is "without angular correlation" (WoAC), i.e. we evaluate the full Hamiltonian of the system but reduce the electron interaction term given in Eq. 3 to $\lambda = 0$. This approximation automatically implies the $S-wave$ approximation for the ground state, since the $(0,0,0)$ configurations are only coupled to any other S configuration $(0, l_1 = l_2, l_2 \neq 0)$ through angular correlation.

However in the final state a complete active space of configurations (L, l_1, l_2) is reduced to the following set: (0,0,0),(0,1,0),(0,0,1),(0,1,1),(2,0,2),(2,2,0),(2,1,1). The results are shown in Fig. 8. The comparison with the full *ab initio* simulations reveal that radial electron correlation already accounts with high accuracy, for the two-photon single ionization paths up to ~ 70 eV, except in the energy region where autoionizing states appears. Indeed, up to the appearance of the first singly excited state, 1s2p at 21.2 eV, the results of the truncated (both the SW-SAe and WoAC) and the *ab initio* simulations are identical. On the other hand, the absence of any trace of autoionization in the $^1\mathrm{D}^e$ symmetry is expected in the WoAC calculation, since only angular correlation can couple the $^1\mathrm{D}^e$ doubly excited state with the background continua associated to the 1s He^+ state. The fact that electron angular correlation is also the major effect that describe autoionization, even for the lowest $^1\mathrm{S}^e$ state, is also clear, because only a reminiscence signature of this state appears in this model.

Therefore, it can be concluded that for photon energies below the ATI-like region the radial correlation plays a dominant role, i.e. the angular correlation terms may be neglected to describe the angular and energy differential observables upon two-photon single ionization. Moreover, as long as a sequential ionization/resonant excitation process occurs, we mostly observe two active uncorrelated electrons. For photon energies populating the doubly excited states, the lack of angular correlation have a huge impact into the asymmetry parameters, and the model is not able to describe even qualitatively the *ab initio* calculations. For higher photon energies, the angular distributions are well described by the model. The most striking results are those for $\omega > 57$ eV, where the highly correlated shake-up processes are possible in a one-photon transition. As can be seen, the angular distributions barely note that angular correlations were turned-off, even though the high electron correlation of the mechanisms involved. Indeed, looking at the clear deviations in this high-energy region for the S-wave single active electron approximation (Fig. 7), it is clear that radial correlation in the ground state is the key term to account for in this region.

VI. CONCLUSIONS

We have provided an analysis of two-photon single ionization of helium for photon energies ranging from threshold to 67 eV. We have shown that the only dependence with pulse duration appears in the low energy region, and vanishes a soon as continuum-continuum transitions are the largest contribution to the second order process. Furthermore, by analyzing the photoelectron angular distributions it is possible to identify distinct mechanisms that govern the two-photon single ionization process: (i) a single active electron behavior in the energy region up to 29 eV, where electron screening is the main effect of the electron correlation terms, (ii) a two-active uncorrelated electrons for photon energies between 32 up to 50 eV, and (iii) highly correlated photoelectron emission for photon energies close to the doubly excited states or reaching the second ionization threshold by one-photon absorption. We have shown that a simple model employing an effective potential can provide accurate values for the β parameters to accurately describe the photoelectron angular distributions in the lowest energy region, and even a simple one-photon transition already accounts for the observed distribution where core-excited resonances dominate the process. We have reported accurate values for the β parameters and angular distributions that change rapidly with energy in the region where doubly excited states are populated, given the rapid change in the S and D ratio for the ionization amplitudes. We analyze how it is possible to observe an almost s- or d-wave behavior at specific energies or how the electron ejection in the light polarization direction can be fully suppressed, resulting into an unexpectedly large electron emission that can appear in the perpendicular plane with respect to the light polarization. It is noticeable that these findings around the autoionizing states are observed, independent of the pulse duration employed to reach them by two-photon absorption, since the continuum-metastable and continuum-continuum transitions are the largest contribution, which behave as mostly independent on the pulse duration.

VII. ACKNOWLEDGMENTS

We acknowledge support from the Ministerio de Economía y Competitividad, through the projects FIS2016-77889-R and FIS2017-92382-EXP, and through the Ramón y Cajal contract from AP. D.B. and O.F. acknowledge financial support from Agencia Nacional de Promoción Científica y Tecnológica, project PICT 2015-3392, and PIP 0784 from Consejo Nacional de Investigaciones Científicas y Técnicas, from Repblica Argentina. Work at LBNL was performed under the auspices of the US DOE under Contract DE-AC02-05CH11231 and was supported by the U.S. DOE Office of Basic Energy Sciences, Division of Chemical Sciences. Simulations performed with computer time allocated at MareNostrum at the Barcelona Computing Center (BSC) through the Spanish Supercomputing Network (RES) with Ref. QCM-2018-2-0033, and in the supercomputer funded by the grant no. 290853 XCHEM from the European Research Council located in the Centro de Computación Científica UAM.

[1] G. S. Voronov and N. Delone, Soviet Physics-JETP Letters **1**, 66 (1965).
[2] P. Agostini, G. Barjot, J. F. Bonnal, G. Mainfray, and C. Manus, IEEE J. Quantum. Electron. **4**, 667 (1968).
[3] G. Mainfray and G. Manus, Reports on Progress in Physics **54**, 1333 (1991).
[4] P. Agostini, F. Fabre, G. Mainfray, G. Petite, and N. K. Rahman, Physical Review Letters **42**, 1127 (1979).
[5] Y. Gontier, M. Poirier, and M. Trahin, Journal of physics B-Atomic molecular optical physics **13**, 1381 (1980).
[6] M. Waitz, R. Y. Bello, D. Metz, J. Lower, F. Trinter, C. Schober, M. Keiling, U. Lenz, M. Pitzer, K. Mertens, M. Martins, J. Viefhaus, S. Klumpp, T. Weber, L. P. H. Schmidt, J. B. Williams, M. S. Schöffler, V. V. Serov, A. S. Kheifets, L. Argenti, A. Palacios, F. Martín, T. Jahnke, and R. Dörner, Nature Communications **8**, 2266 (2017), 1801.03746.
[7] M. S. Pindzola and F. Robicheaux, Journal of Physics B: Atomic, Molecular and Optical Physics **31**, L823 (1998).
[8] L. A. A. Nikolopoulos and P. Lambropoulos, J. Phys. B: Atomic, Molecular and Optical Physics **34**, 545 (2001).
[9] R. Shakeshaft, Phys. Rev. A **76**, 063405 (2007).
[10] H. W. van der Hart and P. Bingham, J. Phys. B: Atomic, Molecular and Optical Physics **38**, 207 (2005).
[11] Y. Kobayashi, T. Sekikawa, Y. Nabekawa, and S. Watanabe, Opt. Lett. **23**, 64 (1998).
[12] L. H. Haber, B. Doughty, and S. R. Leone, Phys. Rev. A **79**, 031401 (2009).
[13] P. O'Keeffe, P. Bolognesi, R. Richter, A. Moise, E. Ovcharenko, L. Pravica, R. Sergo, L. Stebel, G. Cautero, and L. Avaldi, Journal of Physics: Conference Series **235**, 012006 (2010).
[14] L. H. Haber, B. Doughty, and S. R. Leone, Phys. Rev. A **84**, 013416 (2011).
[15] T. Sato, A. Iwasaki, K. Ishibashi, T. Okino, K. Yamanouchi, J. Adachi, A. Yagishita, H. Yazawa, F. Kannari, M. Aoyma, K. Yamakawa, K. Midorikawa, H. Nakano, M. Yabashi, M. Nagasono, A. Higashiya, and T. Ishikawa, Journal of Physics B: Atomic, Molecular and Optical Physics **44**, 161001 (2011).
[16] S. Mondal, H. Fukuzawa, K. Motomura, T. Tachibana, K. Nagaya, T. Sakai, K. Matsunami, S. Yase, M. Yao, S. Wada, H. Hayashita, N. Saito, C. Callegari, K. C. Prince, P. O'Keeffe, P. Bolognesi, L. Avaldi, C. Miron, M. Nagasono, T. Togashi, M. Yabashi, K. L. Ishikawa, I. P. Sazhina, A. K. Kazansky, N. M. Kabachnik, and K. Ueda, Journal of Physics B: Atomic, Molecular and Optical Physics **46**, 205601 (2013).
[17] K. L. Ishikawa and K. Ueda, Phys. Rev. Lett. **108**, 033003 (2012).
[18] K. L. Ishikawa and K. Ueda, Applied Sciences **3**, 189 (2013).
[19] D. Proulx and R. Shakeshaft, Journal of Physics B: Atomic, Molecular and Optical Physics **26**, L7 (1993).
[20] A. Burgers, D. Wintgen, and J. M. Rost, J. Phys. B: Atomic, Molecular and Optical Physics **28**, 3163 (1995).
[21] A. Palacios, C. W. McCurdy, and T. N. Rescigno, Phys. Rev. A **76**, 043420 (2007).
[22] A. Palacios, T. N. Rescigno, and C. W. McCurdy, Physical Review A **77**, 032716 (2008).
[23] C. W. McCurdy, M. Baertschy, and T. N. Rescigno, Journal of Physics B: Atomic, Molecular and Optical Physics **37**, R137 (2004).
[24] S. Balay, S. Abhyankar, M. F. Adams, J. Brown, P. Brune, K. Buschelman, L. Dalcin, A. Dener, V. Eijkhout, W. D. Gropp, D. Kaushik, M. G. Knepley, D. A. May, L. C. McInnes, R. T. Mills, T. Munson, K. Rupp, P. Sanan, B. F. Smith, S. Zampini, H. Zhang, and H. Zhang, "PETSc Web page," `http://www.mcs.anl.gov/petsc` (2018).
[25] A. Palacios, D. A. Horner, T. N. Rescigno, and C. W. McCurdy, Journal of Physics B: Atomic, Molecular and Optical Physics **43**, 194003 (2010).
[26] E. Foumouo, G. L. Kamta, G. Edah, and B. Piraux, Phys. Rev. A **74**, 063409 (2006).
[27] Note that the expression 11 is accurate as long as no intermediate resonant states significantly contribute and, in any case, it becomes exact in the limit of $T \to \infty$. This expression is only used to obtain a magnitude for the total cross section, yet being more accurate that the expression of the cross sections employed in some previous studies [39] performing an integration in energy over the ionization probabilities obtained for a given pulse. In that case the cross section is written as $\sigma(cm^{2N}s^{N-1}) = (\omega/I)^N C(N)^{-1}/TP$, where I is the laser intensity, T the duration and ω the central frequency of the pulse, and $C(N)^{-1}$ is obtained from the long time limit $C(N=2)^{-1} = 128/35$.
[28] T. N. Rescigno and C. W. McCurdy, Phys. Rev. A **62**, 032706 (2000).
[29] G. W. F. Drake, M. M. Cassar, and R. A. Nistor, Phys. Rev. A **65**, 054501 (2002).
[30] U. Fano, Phys. Rev. A **32**, 617 (1985).
[31] U. Fano, Phys. Rev. A **32**, 617 (1985).
[32] I. Sánchez, H. Bachau, and E. Cormier, J. Phys. B: Atomic, Molecular and Optical Physics **28**, 2367 (1995).
[33] A. Saenz and P. Lambropoulos, Journal of Physics B: Atomic, Molecular and Optical Physics **32**, 5629 (1999).
[34] L. Feng and H. W. van der Hart, Journal of Physics B: Atomic, Molecular and Optical Physics **36**, L1 (2003).
[35] A. Palacios, T. N. Rescigno, and C. W. McCurdy, Phys. Rev. A **79**, 033402 (2009).
[36] G. F. Gribakin, V. K. Ivanov, A. V. Korol, and M. Y. Kuchiev, Journal of Physics B: Atomic, Molecular and Optical Physics **32**, 5463 (1999).
[37] F. L. Yip, D. A. Horner, C. W. McCurdy, and T. N. Rescigno, Phys. Rev. A **75**, 042715 (2007).
[38] V. Véniard and B. Piraux, Phys. Rev. A **41**, 4019 (1990).
[39] S. Laulan and H. Bachau, Phys. Rev. A **68**, 013409 (2003).

Appendix A: Details of photoelectron angular distributions

Two-photon single ionization probabilities are plotted as a function of the emission angle and the effective photon energy absorbed indicated in the legends. There is a one-to-one correspondence with the three-dimensional PADs shown in Fig. 2 and discussed in section III. To

reveal important additional detail, cuts in a plane containing the polarization axis are shown in Fig. A.1. The asymmetry in the PADs shown for 15 and 18 eV is due to the interference between one- and two-photon absorption paths. Since one-photon single ionization is orders of magnitude more probable than two-photon single ionization (in the perturbative regime, the N-photon transition probabilities scale with the laser intensity as I^N) and we are using broadband energy pulses (2 fs of duration), it is possible that both one- and two-photon absorption processes emit electrons with the same energy, although different angular momenta. This is the case for 15 and 18 eV. For larger effective photon energies absorbed, i.e. analyzing higher final photoelectron energies, only the two-photon absorption contributes. In the panels of this figure corresponding to 40.8 and 48.38 eV the close resemblance of the PAD to a $\cos^2$ distribution is evident, supporting the assignment of ionization followed by excitation as the dominant mechanism of single ionization in this region.

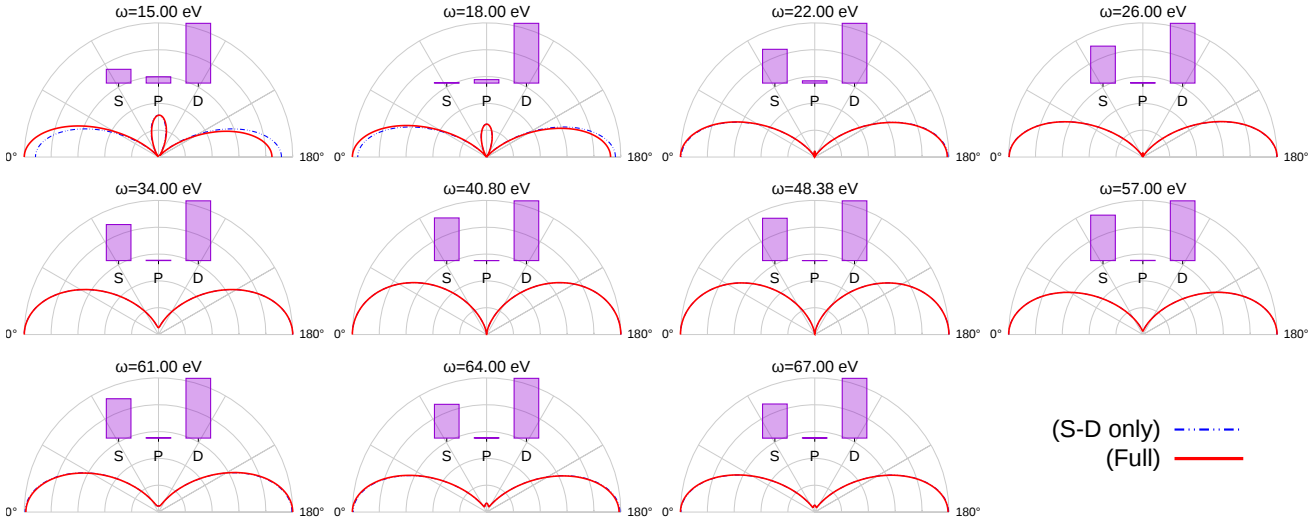

Figure A.1. Photoelectron angular distributions for two photon single ionization of helium. Red full line corresponds to cuts of the three-dimensional distributions in figure 2 taking along the plane that contains the light polarization vector. These are the angular differential probabilities including all ionization channels (S, P and D contributions), i.e. one- and two-photon absorption probabilities are coherently added. Blue dashed line correspond to only the S and D contributions, i.e. only resulting upon a two-photon absorption. Purple bars in each subplot represent the absolute value of the ionization amplitudes associated to the S, P and D contributions.